JOURNAL OF EXPERIMENTAL AND THEORETICAL PHYSICS, 2024, Vol. 166, No. 3 (9), pp. 277–287

ATOMS, MOLECULES, OPTICS

DIFFERENTIATION AND INTEGRATION OF FEMTOSECOND PULSE ENVELOPE USING ONE-DIMENSIONAL PHOTONIC STRUCTURES WITH AN ARTIFICIAL PHOTONIC BANDGAP SHAPE

© 2024 P. S. Emelyantsev, S. E. Svyakhovsky*

Lomonosov Moscow State University, Faculty of Physics 119991, Moscow, Russia

**e-mail: sse@shg.ru*

Received September 11, 2023

Revised January 23, 2024

Accepted January 23, 2024

Abstract. The possibility to create multilayer dielectric structures (photonic crystals) performing integration and differentiation of the first and higher orders of the femtosecond pulse envelope has been shown theoretically. Suggested photonic crystals have a completely artificial photonic bandgap profile, which was achieved by solving the inverse problem of photonic crystals' optical response. The performance of these optical devices in a spectral range wider than an octave has been demonstrated.

Keywords: *photonic crystals, differentiation, integration, femtosecond phenomena, optical pulses*

DOI: 10.31857/S004445102409e013

1. INTRODUCTION

Today, a significant portion of information is transmitted using optical signals, therefore, creating devices for processing optical information directly without conversion to electronic signal is an urgent task. Analog optical signals can undergo mathematical operations such as differentiation and integration [1]. Let us first consider photonic differentiators, whose output optical signal is proportional to the time derivative of the input. There are two main categories of optical differentiators: field differentiators (FD) and intensity differentiators (ID). In ID, both input signals and output differentiated signals are carried by optical intensity or optical power independently of the signal phase, which is useful for ultra-wideband microwave communication and signal encoding [4]. ID can be implemented through nonlinear effects in semiconductor optical amplifiers using incoherent photonic processors [5] of highly nonlinear optical fiber [2].

On the other hand, field differentiation means that the output optical field (complex signal including both amplitude and phase) represents differentiated signals of the input field, which can potentially be applied for ultrashort pulse generation [6, 7], generation of odd-symmetry Hermite–Gaussian signals [8], pulse front recognition [9], and tunable microwave filtering [10]. To date, PDs have been implemented using fiber Bragg gratings [11], phase-shifted Bragg gratings [12, 13], Bloch waves in one-dimensional photonic crystals (PC), long-period fiber gratings [8, 14], interferometers [15], metal-dielectric structures [16], semiconductor optical amplifiers [7, 10], silicon microring resonators [17, 18, 19], and selective directional couplers [20, 21].

An optical temporal differentiator of order N is defined as a device that computes the Nth-order time derivative of the complex envelope of an input optical signal. Such devices can provide more complex temporal signal shapes, such as Hermite–Gaussian functions [22], as these functions are Nth-order derivatives of the Gaussian function. Furthermore, optical signals of arbitrary shape can also be composed from a family of arbitrary-order differentiations of a Gaussian pulse.

The spectral response of an Nth-order differentiator must have an Nth-order zero at the pulse central frequency, which is typically

achieved by adjusting the spectral response parameters of known photonic structures. High-order differentiators have been implemented using cascaded [23], tilted [24], and specially designed fiber Bragg gratings [11], using programmable pulse shapers [25], silicon Bragg gratings [26], two-cascade self-coupled silicon waveguides [27], etc.

It is also worth noting the possibility of implementing photonic differentiators based on Mach–Zehnder interferometers [28, 29]. Such devices can serve as both intensity and field differentiators, depending on the relative shift between the probe wavelength and the resonance mark.

A photonic time integrator of the N-th order (where N=1,2,3... refers to the order of integration) is a device that computes the N-th cumulative time integral of the input signal. Time integrators are fundamental building blocks in many signal processing operations of interest, for example, in computational, control, sensing, and communication networks [30]. Compared to their electronic counterparts, photonic time integrators can provide much greater operating bandwidth, i.e., higher processing speed. First-order photonic time integrators have been proposed for various applications, including ultrafast pulse shaping [31, 32], all-optical memory devices [33, 34], and analog optical computing devices [35, 36]. A relevant example of these devices' application is computational systems designed to solve ordinary differential equations (ODEs). Linear ODEs can be solved in real-time using an appropriate combination of first-order and high-order integrators, adders, and multipliers. Implementation of these operations in an all-optical manner would lead to processing speeds completely unattainable by modern electronic technology.

In recent years, various implementations of photonic time integrators based on different technologies have been widely investigated, for example, using fiber Bragg gratings [37, 38], phase-shifted Bragg gratings [39], resonant diffraction gratings [40], microring resonators [41, 42, 43], temporal spectral convolution systems [44], active Fabry–Perot resonators with semiconductor optical amplifiers as the active medium [45].

It should be noted that despite numerous works in this field, the proposed approaches to solving this problem rely on known spectral properties of various photonic structures, including Bragg structures. For example, to obtain an Nth-order differentiator in [13], a combination of N microresonator modes of a Bragg structure with defects is used. However, this approach has significant limitations since the spectral response of the defect mode in a Bragg structure has a fixed shape that differs from the power law, and only an approximation of the power law dependence can be created from combinations of such responses.

In this work, we use a universal method for constructing the spectral response based on solving the inverse problem [46]. The required spectral response in the form of a power function is artificially created and can have any desired shape. The proposed method makes it possible to implement integrators and differentiators in any spectral range without limitations on its width. The method's applicability is demonstrated for devices with a wide operating range up to an octave and beyond.

2. CALCULATION METHODS

The paper examines field pulse differentiators and integrators. Consider an optical pulse incident on an optical medium at zero angle with the form

$$E_i(r,t) = E_0(t)e^{i(\omega_0 t - kr)}, \quad (1)$$

where $E_0(t)$ is the pulse envelope, $e^{i(\omega_0 t - \mathbf{kr})}$ — oscillations at the pulse central frequency ω_0, whose wave vector in free space is $k = \omega_0 / c$. Since light is incident normally, pulse polarization is not important, and the problem reduces to one dimension.

Let a one-dimensional photonic crystal be defined as a refractive index dependence $n(x)$ on the optical path length, measured from the input face. Using optical path automatically accounts for the refractive index dispersion effect, which simplifies calculations. The complex reflection coefficient spectrum $r(\omega)$ of this PC is calculated using the propagator matrix method [47], where the continuous dependence $n(x)$ was approximated discretely by dividing the medium into layers with optical thickness of 20 nm, which is much smaller than the wavelength and, consequently, the characteristic modulation period. The correctness of this approach was discussed in [48].

The form of the pulse reflected from the crystal is found through Fourier transformation. The spectrum of the original signal envelope

$$E_0(\omega - \omega_0) = \frac{1}{\sqrt{2\pi}} \int_{-\infty}^{\infty} E_0(t) e^{-i\omega t} dt \qquad (2)$$

is multiplied by the reflection coefficient spectrum $r(\omega)$, followed by calculating the inverse Fourier transform:

$$E(t) = \frac{1}{\sqrt{2\pi}} \int_{-\infty}^{\infty} r(\omega) E_0(\omega - \omega_0) e^{i\omega t} d\omega. \qquad (3)$$

The Fourier transform was performed numerically using the fast Fourier transform algorithm, using 8192 points with a time step of 1 fs, frequency step 2.84×10^{11} Hz.

3. PULSE ENVELOPE DIFFERENTIATOR

A signal differentiator can be implemented using the Fourier transform property for function $f(t)$ and its derivative:

$$\frac{d^N f(t)}{dt^N} \leftrightarrow (i\omega)^N f(\omega). \qquad (4)$$

In the case of differentiating the optical pulse envelope $f(t)e^{i\omega_0 t}$, we have

$$\frac{d^N f(t)}{dt^N} \leftrightarrow (i(\omega - \omega_0))^N f(\omega - \omega_0). \qquad (5)$$

Therefore, signal differentiation can be performed using an element whose spectral response equals

$$K_N(\omega) = \alpha (i(\omega - \omega_0))^N.$$

The design and fabrication of such structures presents significant complexity. In this work, we will use the previously developed [46] universal method for constructing multilayer media structures with arbitrary spectral dependence of the reflection coefficient. Applied to the task of constructing specified responses, $K_N(\omega)$ the method is as follows.

Consider the case $N = 1$. Let's construct a photonic crystal whose reflection coefficient spectrum has a linear frequency dependence with a first-order pole in the middle. Let the PC initially be a continuous medium with thickness $D = 100$ μm, refractive index $n_0 = 1.5$ and optical thickness $L = nd = 100$μm. Let's introduce refractive index modulation

$$n_1(x) = A_1 \cos(k_1 x + \varphi_1) + n_0, \qquad (6)$$

where k_1 is the wave number corresponding to frequency ω_1; A_1, φ_1 is the amplitude and phase of the wave. A light wave with wave number $k_1 / 2$ will experience diffractive reflection from the medium with this modulation. The reflection coefficient $r(\omega_1)$ will be proportional to the modulation amplitude A_1, relevant calculations are provided, for example, in [49], and with increasing A_1 coefficient $r(\omega_1)$ will reach the maximum value of 1. To prevent this, the modulation amplitude must be limited from above.

Now let's introduce M spatial harmonics, let their frequencies ω_j be evenly distributed in the considered range, with the middle corresponding to ω_0. Let the amplitude and phase change linearly with the harmonic number j in a certain required spectral range:

$$A_j = \delta n \left(\frac{j}{M} - \frac{1}{2}\right), \quad \varphi_j = \begin{cases} -\frac{\pi}{2}, & j < \frac{N}{2}, \\ \frac{\pi}{2}, & j > \frac{N}{2}, \end{cases} \qquad (7)$$

where δn is the amplitude of refractive index modulation. Let's sum up all modulation harmonics, resulting in the following distribution of refractive index with PC depth:

$$n_I(x) = n_0 + \delta n \sum_{j=1}^{M} \left(\frac{j}{M} - \frac{1}{2}\right) \cos\left(\frac{2\omega_j x}{c} + \varphi_j\right) \qquad (8)$$

The dependence $n_I(x)$ completely defines PC structure. The graph $n(x)$ is shown in Fig.1*a*, it has the form of a sum of harmonic functions with close frequencies, between which beats are observed, with the maximum beats observed approximately in the middle of the crystal.

Let's construct such a PC, choosing $L = 100$ μm, $\delta n = 0.07$, number of harmonics $M = 300$, spectral range from 11,000 to 14,000 inverse centimeters. The middle of the range corresponds to the wave number $k_0 = 12500$ cm^{-1} or wavelength $\lambda_0 = 800$

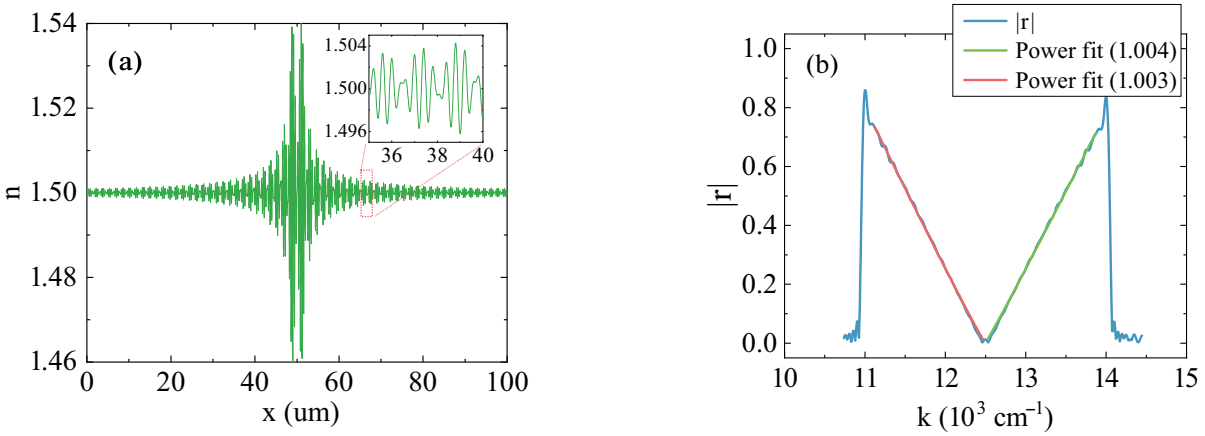

Fig. 1. *a* – PC structure in the form of spatial profile of refractive index $n_I(x)$, with an enlarged fragment of 60-63 μm in the inset,

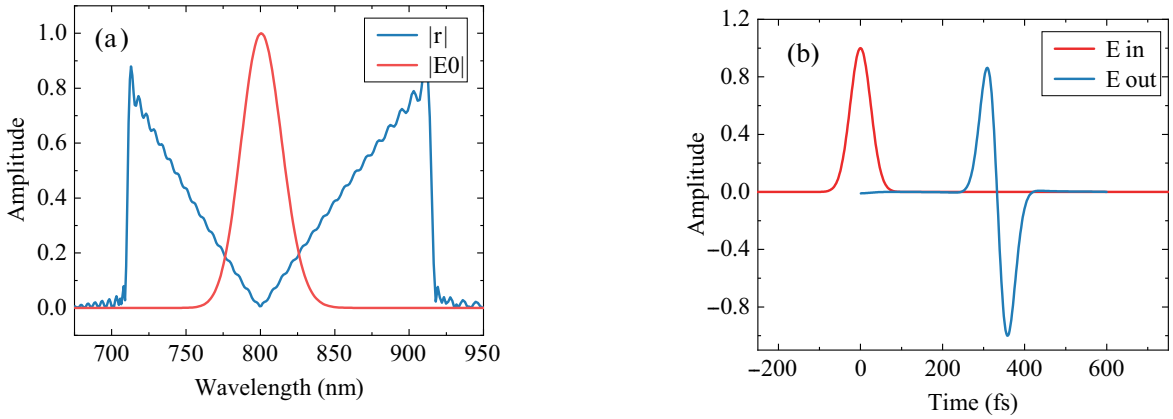

Fig. 2. *a* – Reflection coefficient modulus spectrum compared to incident pulse spectrum, *b* – time profiles of the real part of incident and reflected pulses from this PC

nm. The reflection coefficient spectrum of such PC is demonstrated in Fig.1 *b*. The spectrum has a *V*-shaped form as a function $y = | x |$, the function's zero coincides with the middle of the spectral range.

Spectrum sections that were set as linear functions were approximated by a power function, whose zero corresponded to the wave number $k_0 = 12500$ cm^{-1}. The section from 11,000 to 12,400 cm^{-1} was approximated by function $y = A(k_0 - k)^{\mathsf{a}}$, the section from 12,600 to 14,000 cm^{-1} — by function $y = A(k - k_0)^{\mathsf{a}}$. Approximation results give power indices values nd $\mathsf{a}_1 = 1.003$ and $\mathsf{a}_2 = 1.004$ respectively, which is very close to a linear function.

Let a light pulse with central wavelength of 800 nm and Gaussian envelope of 50 fs duration fall on this PC, its spectrum is shown in Fig. 2*a*, and time profile in Fig. 2*b*. The pulse spectrum falls within the operating range of the PC, with the central pulse frequency corresponding to zero reflection coefficient. The temporal profiles of the reflected and transmitted pulses through the crystal are shown in Fig. 2*b*.

The envelope of the reflected pulse has the form of a first-order Hermite-Gaussian function, which corresponds to the derivative of a Gaussian function. The center of the reflected pulse exits the PC at $t = 334$ fs, corresponding to an optical path of $ct = 100$ μm, thus the pulse is reflected approximately from the middle of the crystal.

For the same structure, $n_I(x)$ let's consider examples of differentiation of other functions. Figure 3 shows calculations of reflected pulses for different shapes of incident pulses. In the case of incident pulses with envelopes in the form of 1st and 5th order Hermite–Gaussian functions, the reflected pulses have envelopes corresponding to 2nd and 6th order Hermite–Gaussian functions respectively. A

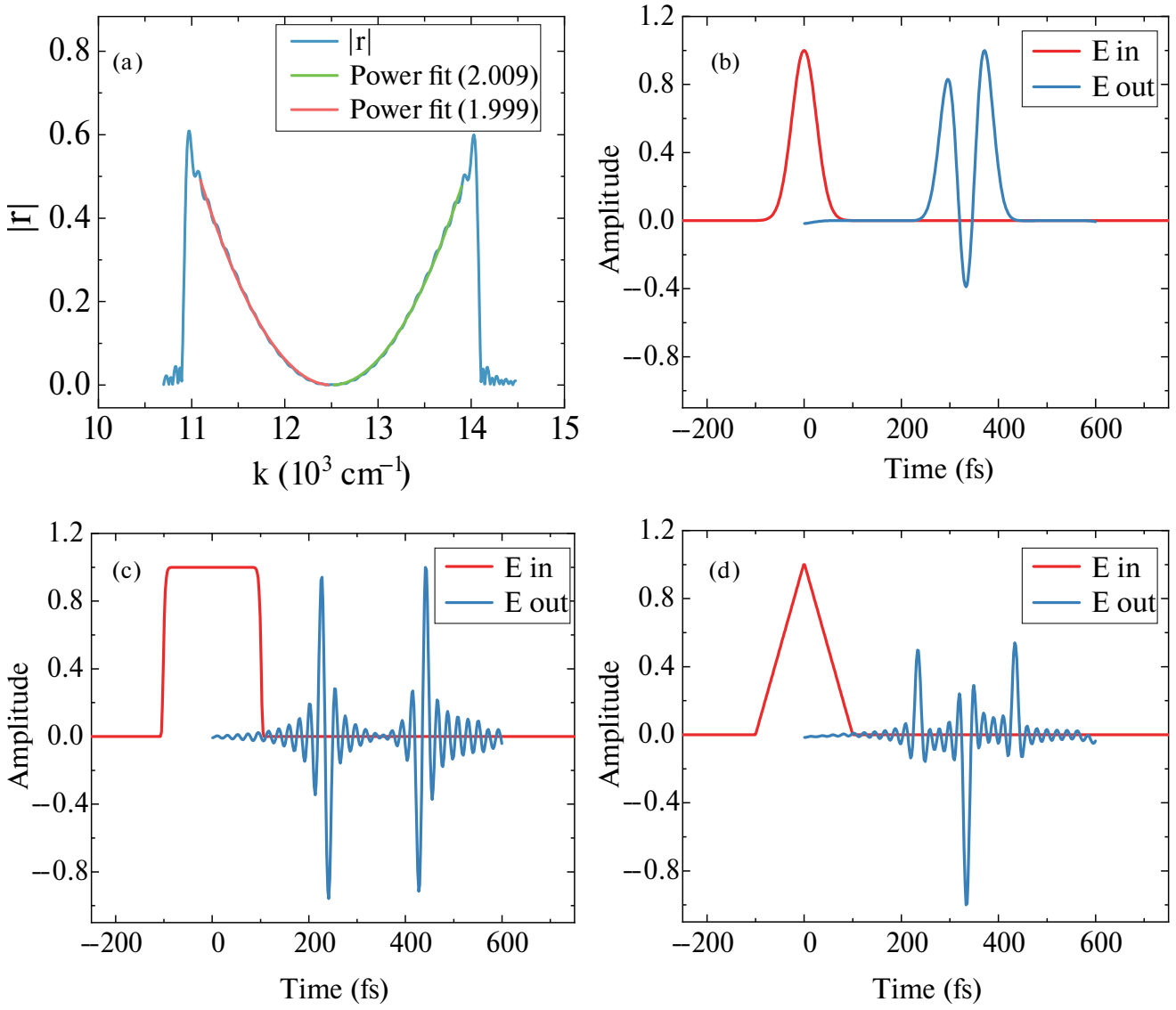

Fig. 3. Temporal profiles of incident and reflected pulses from PC with linearly modulated bandgap. Incident pulses: *a* — 1st order Hermite–Gaussian, *b* — 5th order Hermite-Gaussian, *c* — rectangular, *d* — triangular

rectangular pulse is differentiated in the form of two short peaks of opposite signs, with the time delay between maxima corresponding to the duration of the original pulse. After transformation, a triangular pulse appears as two consecutive U-shaped pulses of different polarity with horizontal sections, whose average amplitude values are 0.56 and 0.67, with pulse deviations from the mean values of horizontal sections not exceeding 17 %.

4. HIGHER-ORDER DIFFERENTIATORS

Let us consider a second-order differentiator. Let the spatial profile of the refractive index have the form

$$n_{II}(x) = n_0 + \Delta n \sum_{j=1}^{M} \left(\frac{j}{M} - \frac{1}{2} \right)^2 \cos\left(\frac{2\omega_j x}{c} + 2\varphi_j \right) \qquad (9)$$

The reflection coefficient spectrum of such PC is shown in Fig. 4*a*. In the region of 11,000–14,000 cm^{-1} it has the form of a quadratic function, the branches of this function were approximated using a power function with zero in the middle of the range. The approximation results show powers of 2.009 and 1.999, which indicates good reproduction of the given quadratic sequence.

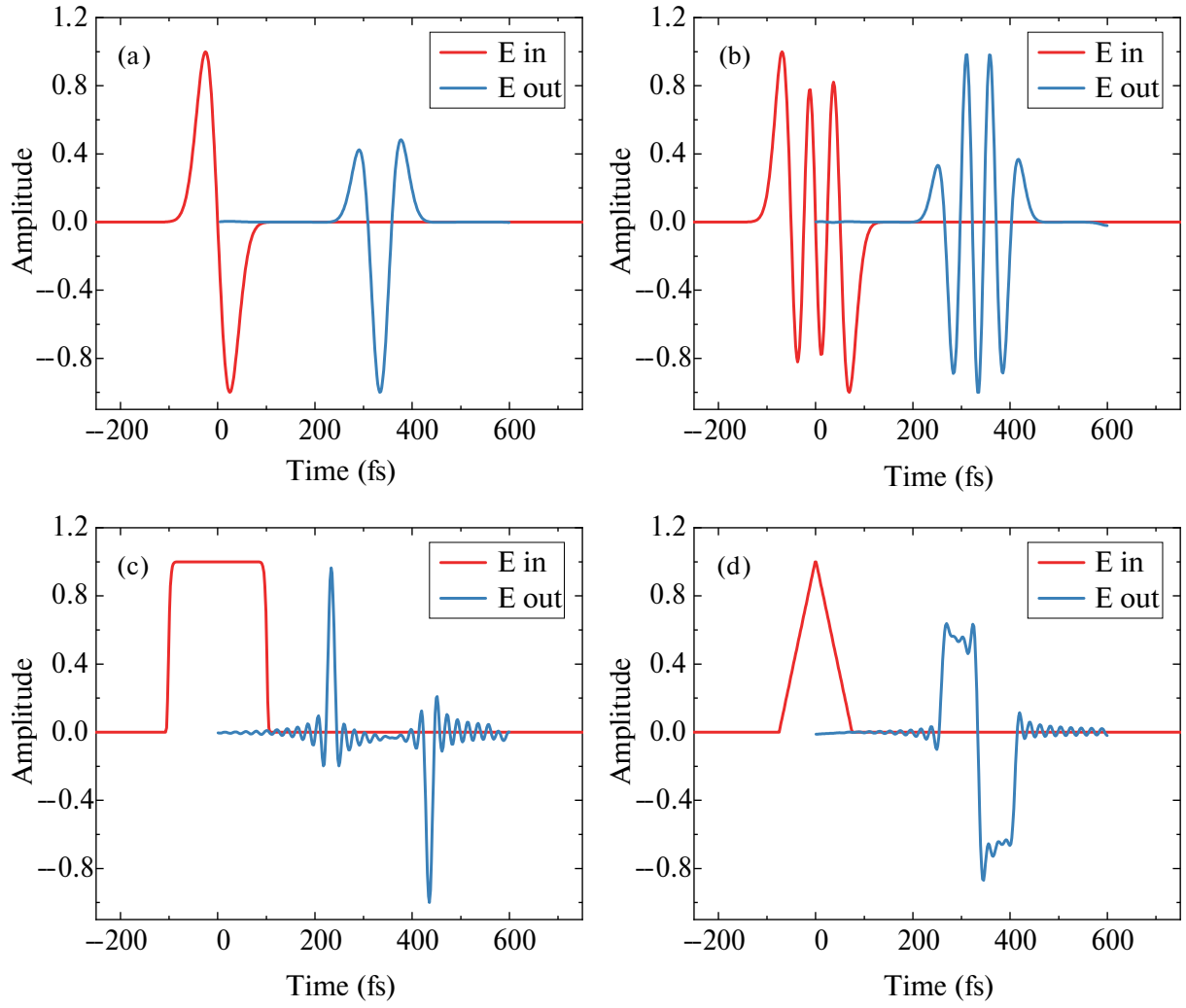

Fig. 4. a – Spectrum of the reflection coefficient module of the PC and approximations of spectrum parts by power functions, b – temporal profiles of the real part of incident and reflected pulses from this PC in case of Gaussian pulse incidence, c – rectangular, d – triangular

The calculated result of reflection of a Gaussian pulse with 50 fs duration and central wavelength of 800 nm = 12500 cm^{-1} is shown in Fig. 4*b*. The shape of the reflected pulse corresponds to the 2nd order Hermite-Gaussian function. As in the case of the first-order differentiator, the center of the reflected signal is also shifted by 330 fs, which corresponds to reflection from the middle of the crystal. In the case of a rectangular pulse (Fig. 4*c*), the response has the form of four sharp peaks corresponding to the derivative of the function shown in Fig. 3*c*. In the case of a triangular pulse, the reflected signal dependence has the form of three peaks, with the middle one having reverse polarity and being twice as large as the outer ones. This corresponds to the derivative of the first derivative of the triangular function (Fig. 3*d*).

Higher-order differentiators (N) can be obtained by constructing a photonic crystal structure of the form

$$n_N(x) = n_0 + \Delta n \sum_{j=1}^{M} \left(\frac{j}{M} - \frac{1}{2} \right)^N \cos\left(\frac{2\omega_j x}{c} + N\varphi_j \right) \quad (10)$$

Figure 5 shows examples of constructing higher-order differentiators and corresponding reflected pulses for the case of a 50 fs Gaussian pulse incidence. All reflected pulse profiles have the number of zeros corresponding to the order of differentiation. However, with increasing order, the magnitude of the first and last maxima decreases, and the envelope

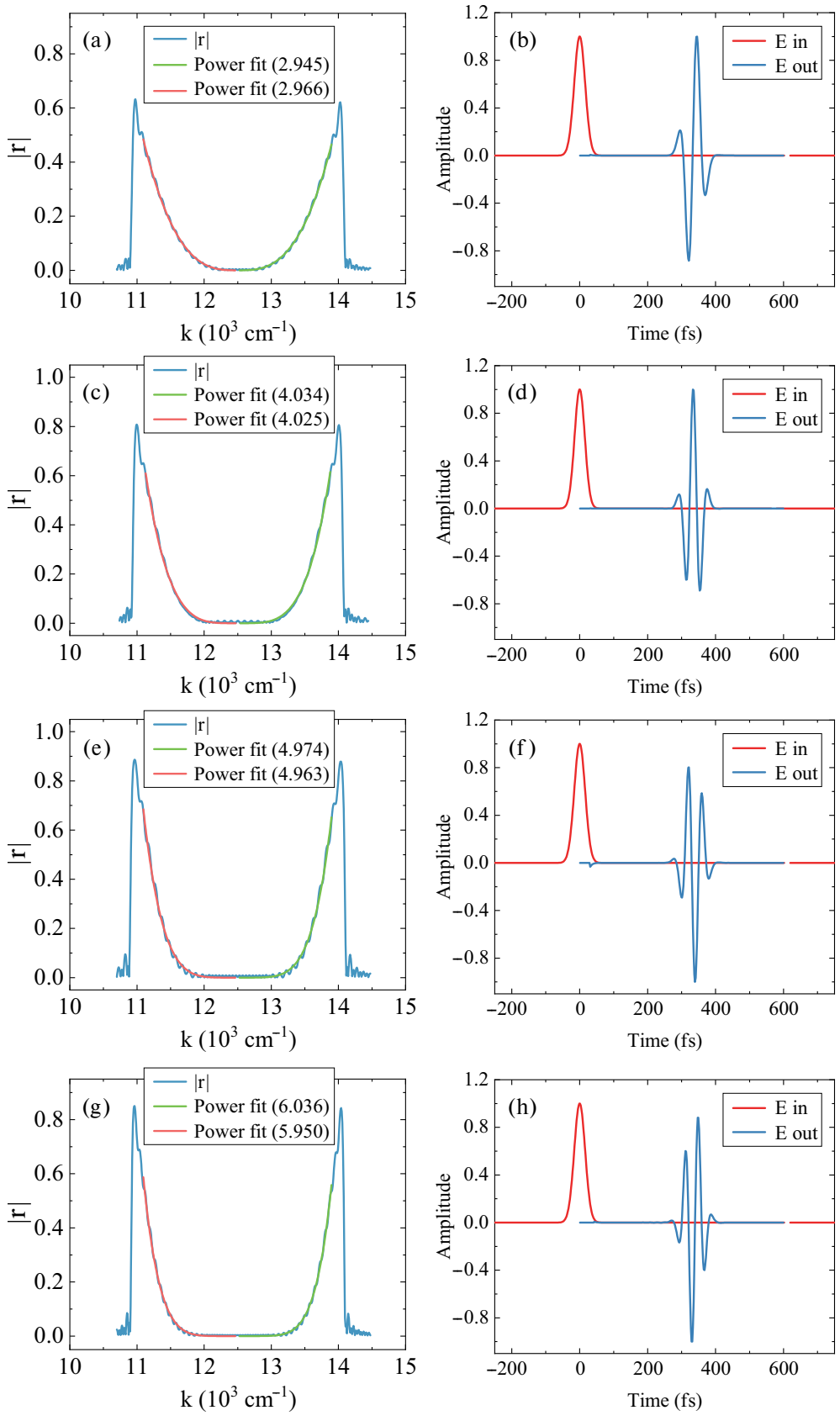

Fig. 5. Spectra of reflection coefficient modulus of PC, approximations of spectrum parts by power functions, and temporal profiles of reflected pulses corresponding to differentiator orders: a, b – 3, c, d – 4, e, f – 5, g, h – 6

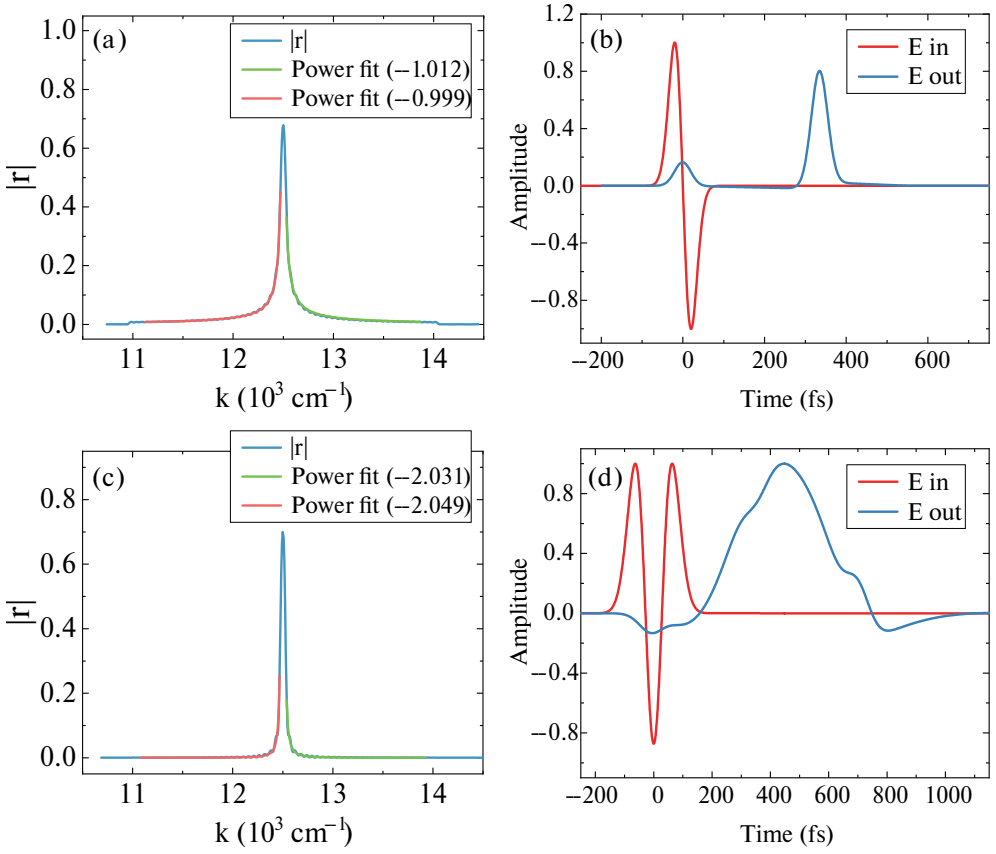

Fig. 6. Spectra of reflection coefficient modulus of PC and approximations of spectrum parts by power functions *a*, *c* and temporal profiles of reflected pulses *b*, *d* demonstrating first and second order integrators

shape differs from the corresponding Hermite–Gaussian function. Therefore, it was decided not to perform further increase in the differentiation order.

5. INTEGRATOR

According to the Fourier transform property for the antiderivative function $F(t) \leftrightarrow (i\omega)^{-1} f(\omega)$, the temporal Nth order integrator of the optical pulse envelope, similar to (5):

$$F^{(N)}(t) \leftrightarrow \frac{1}{(i(\omega - \omega_0))^N} f(\omega - \omega_0) \qquad (11)$$

can be constructed on an optical element whose spectral response has an Nth order pole. Let us construct a photonic crystal with refractive index profile

$$n(x) = n_0 + \sum_{j=1}^{M} \left(\frac{i}{M} - \frac{1}{2} \right)^N \cos\left(\frac{2\omega_j x}{c} - N\varphi_j \right) \qquad (12)$$

The reflection coefficient spectrum of this PC is shown in Fig. 6*a*. The spectrum of PC with a second-order pole in the spectral response is shown in Fig 6*c*. The corresponding power function approximations are shown in the graphs, with power indices converging well with the input data. As input pulses for integration tasks Hermite-Gaussian functions of first and second orders were chosen. Their antiderivative is expected to be in the form of a Gaussian function. The first-order antiderivative is shown in Fig. 6*b*, its shape well reproduces the Gaussian function. The second-order antiderivative is shown in Fig. 6*d*. It can be seen that the function very roughly repeats the Gaussian pulse, and there is also significant pulse broadening in time. Therefore, further increase in the antiderivative order was not conducted.

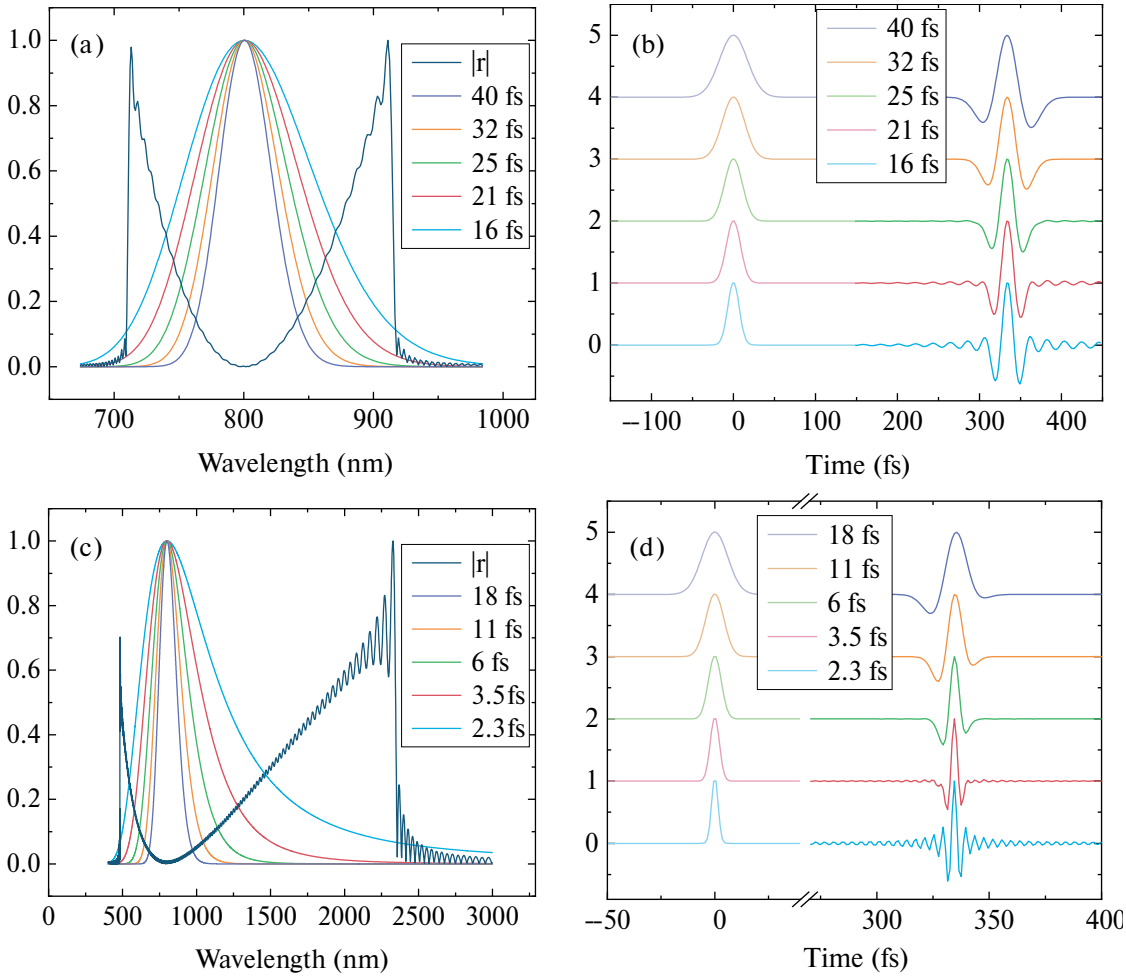

Fig. 7. Spectral responses of second-order differentiators with center frequency 12500 $cm^{-1}$and operating bandwidth 3125 cm^{-1} (*a*) and and 16400 cm^{-1} (*c*) their corresponding temporal profiles of incident (*b*) (b) and reflected (*d*) pulses

6. OPERATING RANGE

The proposed devices perform pulse transformation using spectral modulation, so it is important to determine their operating spectral range. As an example, let's take the considered second-order differentiator of the form $n_{II}(x)$. Let pulses with full width at half maximum field from 16 to 40 fs fall on it. Their spectra in comparison with the PC spectrum are shown in Fig.7*a*, the corresponding temporal profiles of incident and reflected pulses are shown in Fig. 7*b*. For clarity, the spectra are given in nanometers, so the spectrum of the reflection coefficient, which depends parabolically on the wave number, appears distorted.

As the pulse duration decreases from 40 to 16 fs, the pulse spectrum broadens, its edges extend beyond the PC operating range. This leads to parasitic oscillations that are visible in the temporal profile of the reflected pulse. The pulse duration of 25 fs in this demonstration is selected so that the amplitude level of parasitic oscillations reaches 1% by field, and duration of 16 fs. 10 % by field and 1% by intensity. These durations correspond to spectral widths of pulses 583 and 890 cm^{-1}, thus, to avoid parasitic oscillations, it is necessary to choose the operating range wider than the pulse spectrum by 5.3 and 3.5 times respectively.

Now let's expand the operating range to 16400 cm^{-1}, i.e., the range extends from 4300 to 20700 cm^{-1}, which is wider than an octave in frequency.

Fig. 7*c* shows the reflection coefficient spectrum for this range to 1. Let pulses with durations varying from 2.3 to 18 fs fall on the PC (Fig. 7*d*). Parasitic oscillations appear at a duration of 3.5 fs (spectrum width 6233^{-1}), further reduction in duration leads

to strong distortion in calculations. This is due to the fact that the optical cycle duration at 800 nm wavelength is 2.67 fs, and reducing the duration below this value violates the assumption about the existence of the pulse envelope.

7. CONCLUSION

Based on the presented calculations, for the considered PCs, it is necessary to continuously vary the refractive index $n(x)$ with a spatial period of about half the wavelength, create structures up to 100 μm thick, and ensure the absence of significant absorption or scattering after passing through such thickness. This can be implemented in PCs fabricated using anodic aluminum and titanium oxide, as well as two-photon laser lithography. It is known [50] that PCs based on oxidized porous silicon allow the fabrication of structures with the required size and period modulation magnitude.

In this work, methods for constructing photonic crystals that implement mathematical operations of differentiation from first to sixth orders, as well as first and second-order integration, performed on femtosecond pulse envelopes in time, were theoretically demonstrated. The maximum achievable pulse spectrum width was investigated, and it was shown that the proposed approach allows the fabrication of differentiators with a bandwidth of more than an octave.

FUNDING

This work was financially supported by the Russian Science Foundation, project 21- 72-10103, https://rscf.ru/project/21-7210103/ .

REFERENCES

1. D. Bykov, L. Doskolovich, and V. Soifer, Journal of Experimental and Theoretical Physics 114, 724 (2012).

2. P. Velanas, A. Bogris, A. Argyris, and D. Syvridis, Journal of Lightwave Technology 26(18), 3269 (2008).

3. J. Xu, X. Zhang, J. Dong, D. Liu, and D. Huang, Opt. Lett. 32, 1872 (2007).

4. J. Dong, Y. Yu, Y. Zhang, X. Li, D. Huang, and X. Zhang, Opt. Express 19(11), 10587 (2011).

5. Y. Park, M. H. Asghari, R. Helsten, and J. Azana, IEEE Photonics Journal 2(6), 1040 (2010).

6. N. Ngo, S. Yu, S. Tjin, and C. Kam, Optics Communications 230(1), 115 (2004).

7. Z. Li and C. Wu, Opt. Lett. 34(6), 830 (2009).

8. R. Slavık, Y. Park, M. Kulishov, R. Morandotti, and J. Azana, Opt. Express 14(22), 10699 (2006).

9. J. Dong, X. Zhang, S. Fu, J. Xu, P. Shum, and D. Huang, IEEE Journal of Selected Topics in Quantum Electronics 14(3), 770 (2008).

10. X. Li, J. Dong, Y. Yu, and X. Zhang, IEEE Photonics Technology Letters 23(5), 308 (2011).

11. L. M. Rivas, K. Singh, A. Carballar, and J. Azana, IEEE Photonics Technology Letters 19(16), 1209 (2007).

12. N.K. Berger, B. Levit, B. Fischer, M. Kulishov, D. V. Plant, and J. Aza˜na, Optics express 15(2), 371 (2007).

13. M. Kulishov and J. Aza˜na, Optics Express 15(10), 6152 (2007).

14. R. Slav′ık, Y. Park, M. Kulishov, and J. Azana, Opt. Lett. 34(20), 3116 (2009).

15. Y. Park, J. Aza˜na, and R. Slavık, Opt. Lett. 32(6), 710 (2007).

16. L. L. Doskolovich, A. I. Kashapov, E. A. Bezus, and D. A. Bykov, Photonics and Nanostructures-Fundamentals and Applications 52, 101069 (2022).

17. F. Liu, T. Wang, L. Qiang, T. Ye, Z. Zhang, M. Qiu, and Y. Su, Opt. Express 16(20), 15880 (2008).

18. Y. Hu, L. Zhang, X. Xiao, Z.-Y. Li, Y. Li, T. Chu, Y. Su, Y. Yu, and J. Yu, Journal of Optics 14 (2012).

19. J. Dong, A. Zheng, D. Gao, S. Liao, L. Lei, D. Huang, and X. Zhang, Opt. Lett. 38(5), 628 (2013).

20. T. L. Huang, A. L. Zheng, J. J. Dong, D. S. Gao, and X. L. Zhang, Opt. Lett. 40(23), 5614 (2015).

21. T.-J. Ahn and J. Aza˜na, Opt. Express 19(8), 7625 (2011).

22. Y. Park, M. Kulishov, R. Slavık, and J. Azana, Opt. Express 14(26), 12670 (2006).

23. L. M. Rivas, S. Boudreau, Y.Park, R. Slavık, S. LaRochelle, A. Carballar, and J. Azana, Opt. Lett. 34(12), 1792 (2009).

24. M. Li, L.-Y. Shao, J. Albert, and J. Yao, IEEE Photonics Technology Letters 23(4), 251 (2011).

25. Y. Yu, F. Jiang, H. Tang, L. Xu, X. Liu, J. Dong, and X. Zhang, Opt. Express 24(11), 11739 (2016).

26. K. Rutkowska, D. Duchesne, M. Strain, R. Morandotti, M. Sorel, and J. Azana, Opt. Express 19(20), 19514 (2011).

27. L. Zhang, J. Wu, X. Yin, X. Sun, P. Cao, X. Jiang, and Y. Su, IEEE Photonics Journal 6(2), 1 (2014).

28. J. Dong, A. Zheng, D. Gao, L. Lei, D. Huang, and X. Zhang, Opt. Express 21(6), 7014 (2013).

29. S.Yan, Z. Cheng, L. H. Frandsen, Y. Ding, F. Zhou, J. Dong, and X. Zhang, Opt. Lett. 42(8), 1596 (2017).

30. R. Slavık, Y. Park, N.Ayotte, S. Doucet, T.-J. Ahn, S. LaRochelle, and J. Azana, Opt. Express 16(22), 18202 (2008).

31. N. Q. Ngo, Appl. Opt. 45(26), 6785 (2006).

32. A. Karimi, A. Zarifkar, and M. Miri, J. Lightwave Technol. 38(8), 2346 (2020).

33. Y. Ding, X. Zhang, X. Zhang, and D. Huang, Optics Communications 281(21), 5315 (2008).

34. M. H. Asghari and J. Aza˜na, IEEE Photonics Technology Letters 23(4), 209 (2011).

35. Y. Park, T.-J. Ahn, Y. Dai, J. Yao, and J. Azana, Opt. Express 16, 17817 (2008).

36. J.Azana, IEEE Photonics Journal 2(3), 359 (2010).

37. A. Mohammad H., W. Chao, Y. Jianping, and J. Azana, Opt. Lett. 35(8), 1191 (2010).

38. M. H. Asghari, Y. Park, and J. Aza˜na, Opt. Express 19(2), 425 (2011).

39. N.V. Golovastikov, D.A. Bykov, L. L. Doskolovich, and E. A. Bezus, Optics Communications 338, 457 (2015).

40. D. A. Bykov, L. L. Doskolovich, and V. A. Soifer, JETP Letters 95, 6 (2012).

41. W. Liu, M. Li, R.S. Guzzon, E.J. Norberg, J. S.Parker, L. A. Coldren, and J. Yao, Journal of Lightwave Technology 32(20), 3654 (2014).

42. M. Ferrera, Y. Park, L. Razzari, B. Little, S. Chu, R. Morandotti, D. Moss, and J. Aza˜na, Nature Communications 1, 29 (2010).

43. M. Ferrera, Y. Park, L. Razzari, B. E. Little, S. T. Chu, R. Morandotti, D. J. Moss, andJ. Azana, Opt. Express 19(23), 23153 (2011).

44. A. Malacarne, R. Ashrafi, M. Li, S. LaRochelle, J. Yao, and J. Aza˜na, Opt. Lett. 37(8), 1355 (2012).

45. N. Huang, M. Li, R. Ashrafi, L. Wang, X. Wang, J. Azana, and N. Zhu, Opt. Express 22(3), 3105 (2014).

46. P. Emeliantsev, N. Pyshkov, and S. Svyakhovskiy, JETP Letters 117(11), 821 (2023).

47. A. Luce, A. Mahdavi, F. Marquardt, and H. Wankerl, JOSA A 39(6), 1007 (2022).

48. P. Baumeister, Applied optics 25(16), 2644 (1986).

49. S. Svyakhovskiy and N. Pyshkov, Moscow University Physics Bulletin 78(4), 484 (2023).

50. S. Svyakhovskiy and N. Pyshkov, Optics and Spectroscopy 131(8), 1070 (2023).